An analytic study of the perpendicularly propagating electromagnetic drift instabilities in the Magnetic Reconnection Experiment

Yansong Wang, Russell Kulsrud, and Hantao Ji
Princeton Plasma Physics Laboratory, Princeton, New Jersey 08549, USA

(Received 24 March 2008; accepted 29 October 2008; published online 10 December 2008)

A local linear theory is proposed for a perpendicularly propagating drift instability driven by relative drifts between electrons and ions. The theory takes into account local cross-field current, pressure gradients, and modest collisions as in the Magnetic Reconnection Experiment [M. Yamada *et al.*, Phys. Plasmas **4**, 1936 (1997)]. The unstable waves have very small group velocities in the direction of the pressure gradient, but have a large phase velocity near the relative drift velocity between electrons and ions in the direction of the cross-field current. By taking into account the electron-ion collisions and applying the theory in the Harris sheet, we establish that this instability could be excited near the center of the Harris sheet and have enough e-foldings to grow to large amplitude before it propagates out of the unstable region. Comparing with the other magnetic reconnection related instabilities (lower-hybrid-drift instability, modified two-stream instability, etc.) studied previously, we believe the instability we found is a favorable candidate to produce anomalous resistivity because of its unique wave characteristics, such as electromagnetic component, large phase velocity, and small group velocity in the cross-current-layer direction. © *2008 American Institute of Physics*. [DOI: 10.1063/1.3035907]

I. INTRODUCTION

Magnetic reconnection is a fundamental process whereby magnetic field lines are broken and rejoined in an electric current singularity. In nature, magnetic reconnection proceeds much faster than the predictions of the Sweet–Parker model. Its origin has been a puzzle for many years. Fast reconnection has also been observed in the Magnetic Reconnection Experiment (MRX).[1] Thus, we hope that gaining an understanding of fast reconnection in this experiment will lead to insights into the general problem. There are two main candidate mechanisms in explaining fast reconnection. One is based on the two-fluid effects, which facilitate the separation of electron and ion flows in a laminar fashion, as verified in the MRX.[2] The other one is based on resistivity enhancement due to turbulence within the current sheet.[3] Electromagnetic fluctuations have been measured and have shown positive correlations with fast reconnection in the MRX.[4] These fluctuations may play an important role and speed up the rate of reconnection by enhancing plasma resistivity.

In the current sheet, there are many sources of free energy, such as relative drifts between ions and electrons, pressure gradient, and magnetic field gradient. These could drive instabilities and the resulting turbulence can increase the forces on the current carrying particles and produce an anomalously large resistivity. The lower-hybrid-drift instability[5–22] (LHDI), which is driven by the density gradient, has been extensively studied as a favorable candidate to produce anomalous resistivity in the current sheet. Most of the theories of this instability are based on either the electrostatic approximation assuming very small plasma beta,[8] or local calculations assuming a small density gradient.[13] However, the location where an anomalous resistivity is needed is the center of the current sheet where the local plasma beta is large because of weak magnetic field and large plasma pressure. Also, because of the narrowness of the current sheet (which is order of the ion skin depth), a small density gradient is not an appropriate assumption in most cases.

Most of the previous LHDI theories are only concerned with collisionless plasma and rely on the finite electron Larmor radius effect (finite $k_\perp \rho_e$), because the modes are stable or slowly growing when $k_\perp \rho_e$ is very small.[13] In MRX plasmas where the fluctuations are observed, the electron-electron (e-e) and electron-ion collisions are relatively frequent. These collisions can damp the instabilities requiring large $k_\perp \rho_e$ since the collisional damping effect is proportional to $\nu_{ei} k^2$. No LHDI theory is found to take these effects into account. A viable theory needs also to answer the following questions: What are the driving force for the instability? What are their signatures? How do they grow and saturate? How do they affect the magnetic reconnection process?

Much effort has been devoted to searching for fluctuations in the MRX that produce anomalous resistivity. Electrostatic fluctuations were first found by Carter.[8] However, it turns out these fluctuations only exist on the edge of the current sheet and do not correlate well in time with the reconnection process. These electrostatic fluctuations may have some indirect effects on the reconnection process, such as making the current layer thinner and triggering fast reconnection as suggested by some simulations. But they are not directly related to the anomalous resistivity in the central body of the current sheet. (We note that there are several typos on signs in Carter's calculation, but the plot of the growth rate of the electrostatic LHDI is correct.) Later, Ji,[4] measured electromagnetic fluctuations which are present in the center of the current sheet and correlate in time with the reconnection progress. They have a phase velocity comparable to the relative drift velocity between electrons and ions.

Motivated by these observations, Ji and his colleagues developed a local linear electromagnetic instability in the lower hybrid frequency range.[23] This is an obliquely propagating electromagnetic drift instability. This instability has an appreciable growth rate and could arise near the center of the current sheet. It is driven by a large density gradient. However, when applying this theory to the Harris sheet, we find this instability also has a large group velocity in the direction of the density gradient and it propagates out of the unstable region before it barely e-folds once or twice. In addition, the phase velocity of this instability is much smaller than the experimental measured value.

Since the obliquely propagating instability does not grow to a desirable amplitude in the Harris sheet, we reinvestigate the perpendicularly propagating modes using the same local linear electromagnetic theory. Surprisingly, we find a more favorable instability which has a very small group velocity in the density gradient direction. It has a phase velocity comparable to the relative drift velocity between electrons and ions which is comparable to the experimental measurement. By adding electron-ion collisions and applying the theory in the Harris sheet, we confirm that this instability can still exist in the center of the current sheet where the plasma beta is large. In addition, because of its extremely small group velocity across the current layer, this perpendicularly propagating electromagnetic instability may have sufficient e-foldings to grow to a desired amplitude so that nonlinear effects are important and lead to a resistivity increase.

First, in Sec. II, we present the theoretical calculations of our model. In Sec. III, we discuss the wave characteristics and physical mechanism. In Sec. IV, we apply the theory to the Harris sheet. In Sec. V, we present the modified theory including modest electron-ion collisions. Finally, in Sec. VI, we present our conclusions.

In Appendixes A and B, we revisit the obliquely propagating instability and show why that instability is less favorable than the perpendicularly propagating instability.

II. THEORETICAL MODEL

A. Assumptions and method of the calculation

Because we are trying to explain the observed instabilities in the MRX, we make the same assumptions proposed in previous paper.[23] Namely, we assume that the frequency of the modes is larger than the ion cyclotron frequency and smaller than the electron cyclotron frequency. We also assume that the wavelength is small compared with the ion gyration radius and large compared with the electron gyration radius. Thus, we consider the ions to be unmagnetized, and treat the electrons as a fluid. As we discussed in Sec. I, we neglect the finite $k_\perp \rho_e$ effect, because the electron-ion collision rate in the MRX is relatively high, and they may damp the instabilities at large $k_\perp$.

Since the e-e collision rate in the MRX is comparable to the frequencies of the mode, an isotropic pressure tensor should be a reasonable assumption. Further, we assume the electron pressure is either isothermal or adiabatic based on the experimental data. We also assume T_i and T_e are constant. The Debye length is very small in the MRX even compared with the electron gyration radius, so charge neutrality is a very good approximation. This gives us the perturbed electron density directly in terms of the perturbed ion density.

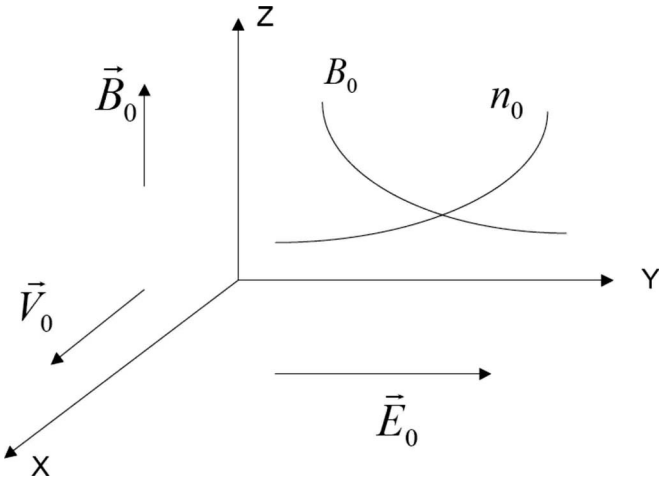

FIG. 1. The equilibrium state. Electrons drift toward the positive x direction and ions are at rest. The unperturbed magnetic field is in the z direction. Pressure gradient and electric field are in the y direction. The positive y direction points toward the center of the current layer.

We take the equilibrium in the MRX to be a Harris equilibrium and study the instability in the frame in which the ions are at rest and the electrons have a diamagnetic drift velocity $\mathbf{V}_0$. As shown in Fig. 1, we take a local Cartesian coordinate system with z along $\mathbf{B}_0$, y in the direction of increasing plasma pressure, and x in the direction of the electron drift. Thus, the electric field balancing the ion pressure force is $\mathbf{E}_0 = E_0 \hat{\mathbf{y}}$, and in the equilibrium,

$$en_0 E_0 = T_i \frac{\partial n_0}{\partial y}, \tag{1}$$

$$-en_0(E_0 - V_0 B_0) = T_e \frac{\partial n_0}{\partial y}. \tag{2}$$

Adding Eqs. (1) and (2), we have $en_0 V_0 B_0 = (T_i + T_e) \times (\partial n_0 / \partial y)$, and

$$E_0 = \frac{T_i}{T_e + T_i} V_0 B_0. \tag{3}$$

Defining $dn_0/dy = \epsilon n_0$, we get

$$\epsilon = \frac{eV_0 B_0}{T_i + T_e}, \tag{4}$$

which is the local relation between the electron drift velocity and the density gradient.

We obtain the perturbed ion density and current from the unmagnetized ion dynamics. The detailed calculation presented in previous paper[23] yields

$$\mathbf{j}^i = -i \frac{n_0 e^2}{M k v_i} [Z(\zeta)\mathbf{E} - (\zeta Z' + Z)(\mathbf{E} \cdot \hat{\mathbf{k}})\hat{\mathbf{k}} + i(\epsilon/k)(\zeta Z' + Z) E_y \hat{\mathbf{k}}], \tag{5}$$

$$n \approx i\frac{n_0 e}{Mk^2 v_i^2} Z'(\zeta)(\mathbf{k}\cdot\mathbf{E} - i\epsilon E_y), \tag{6}$$

where $\hat{\mathbf{k}}=\mathbf{k}/k$, $\zeta=\omega/(kv_i)$, $v_i=\sqrt{2T_i/M}$, and Z is the plasma dispersion function.

We first take the cold ion limit because the unstable modes have a very large phase velocity compared with the ion thermal velocity. We have

$$\mathbf{j}^i \approx i\frac{\omega_{pi}^2}{\omega}\epsilon_0 \mathbf{E}, \tag{7}$$

$$n \approx i\frac{n_0 e}{M\omega^2}(\mathbf{k}\cdot\mathbf{E} - i\epsilon E_y), \tag{8}$$

where $\omega_{pi}\equiv\sqrt{n_0 e^2/M\epsilon_0}$. Later, we will include ion thermal motion.

We obtain the perpendicular electron current from the first-order force for the electron fluid, assuming either an isotropic or adiabatic perturbed pressure. Neglecting the electron inertia term, we have

$$\mathbf{j}^e \times \mathbf{B}_0 = en_0 V_0 \times \mathbf{B} + en_0\mathbf{E} + en\mathbf{E}_0 + \hat{\gamma}\nabla(nT_e). \tag{9}$$

The x and y components of Eq. (9) are given by

$$j_y^e B_0 - i\hat{\gamma}k_x T_e n_1 - n_0 e E_x = 0, \tag{10}$$

$$-j_x^e B_0 + en_0 V_0 B_z - en_1 E_0 - en_0 E_y - \hat{\gamma}(ik_y + \epsilon)T_e n_1 = 0. \tag{11}$$

Here, by taking $\hat{\gamma}=1$ or $5/3$, we have either an adiabatic or isothermal perturbed pressure, depending on the plasma parameters. When the electron mean free path is much smaller than the distance for lines to leave the current layer, [the modes propagate only perpendicularly to the unperturbed magnetic field $(k_\parallel=0)$], there is no heat transport along the field lines to smooth out the temperature. Thus, the temperature perturbations are not zero $[T_1/T_0=(2/3)n_1/n_0]$. After taking into account these temperature perturbations, the factor in front of the perturbed pressure gradient $\hat{\gamma}$ is $5/3$. However, if the electron mean free path is comparable with the length of the current layer, the isothermal pressure assumption is reasonable, with $\hat{\gamma}=1$.

Another important term we must keep is the ϵ term in Eq. (11). This arises from the equilibrium density gradient ϵ. It is important because it gives out-of-phase terms which have the potential to generate instabilities.

We assume that the electric field has a normal mode decomposition proportional to $\exp[i(\mathbf{k}\cdot\mathbf{x}-wt)]$. This is consistent with local theory when wavelengths in the y direction are smaller than the thickness of the current layer. However, other quantities have an additional dependence on y because of the pressure gradient of the equilibrium in y. With the wave vector $\mathbf{k}=(k_x,k_y,0)$, Ampère's law and Faraday's law are combined to give Maxwell equation

$$\mathbf{k}\times(\mathbf{k}\times\mathbf{E}) = -i\omega\mu_0\mathbf{j}. \tag{12}$$

Taking only the perpendicular components, this equation becomes

$$k_y^2 E_x - k_x k_y E_y = i\omega\mu_0 j_x, \tag{13}$$

$$k_x^2 E_y - k_x k_y E_x = i\omega\mu_0 j_y. \tag{14}$$

After calculating the perpendicular x and y electron currents from Eqs. (13) and (14), we can substitute them and the ion currents into Maxwell's equations to find the two independent relations for the perpendicular electric field. The warm ion effects based on Eq. (5) and (6) will be discussed in Sec. IV. Since the parallel electric field is zero, we need only two equations for E_x and E_y. This gives a 2×2 matrix, whose determinant gives the dispersion relation. We are now in a position to write down the equations for E_x and E_y and solve for the dispersion relation.

B. Dispersion relation

Substituting for n_1, $\mathbf{j}^e$ and $\mathbf{j}^i$ [from Eqs. (8), (10), (11), and (7)] into Eqs. (13) and (14), and introducing dimensionless variables, we get

$$\begin{pmatrix} D_{xx} & D_{xy} \\ D_{yx} & D_{yy} \end{pmatrix}\begin{pmatrix} E_x \\ E_y \end{pmatrix} = 0, \tag{15}$$

where

$$D_{xx} = 1 + K_y^2 - \tau\frac{K_x V}{\Omega} + iVK_y - i\hat{\gamma}\frac{\beta_e}{2}\frac{K_x(K_y - i\mathcal{E})}{\Omega},$$

$$D_{xy} = i(\Omega - K_x V) - \tau\frac{K_y - i\mathcal{E}}{\Omega}V - i\hat{\gamma}\frac{\beta_e}{2}\frac{(K_y - i\mathcal{E})^2}{\Omega} - K_x K_y,$$

$$D_{yx} = i\hat{\gamma}\frac{\beta_e}{2}\frac{K_x^2}{\Omega} - i\Omega - K_x K_y,$$

$$D_{yy} = 1 + K_x^2 + i\hat{\gamma}\frac{\beta_e}{2}\frac{K_x(K_y - i\mathcal{E})}{\Omega}.$$

The dimensionless parameters are defined by

$$\Omega \equiv \frac{\omega}{\omega_{ci0}}, \quad K \equiv k\frac{c}{\omega_{pi0}}, \quad \mathcal{E} \equiv \epsilon\frac{c}{\omega_{pi0}}, \quad V \equiv \frac{V_0}{V_{A0}},$$

$$\beta_e \equiv \frac{n_0 T_e}{B_0^2/2\mu_0}, \quad \beta_i \equiv \frac{n_0 T_i}{B_0^2/2\mu_0}, \quad \tau \equiv \frac{T_i}{T_e + T_i}, \tag{16}$$

and

$$\hat{\gamma} = \begin{cases} 5/3, & \text{for adiabatic process,} \\ 1, & \text{for isothermal process.} \end{cases}$$

Here,

$$\omega_{ci0} \equiv \frac{B_0 e}{M}, \quad V_{A0} \equiv \frac{B_0}{\sqrt{\mu_0 M n_0}}, \quad \omega_{pi0} \equiv \sqrt{\frac{n_0 e^2}{M\epsilon_0}}. \tag{17}$$

We note here that in the parallel (z) direction, there is only a simple drift wave $\Omega=K_x V$ decoupling from the waves described by the 2×2 matrix. Setting the determinant of the matrix equal to zero,

$$D_{xx}D_{yy} - D_{xy}D_{yx} = 0. \tag{18}$$

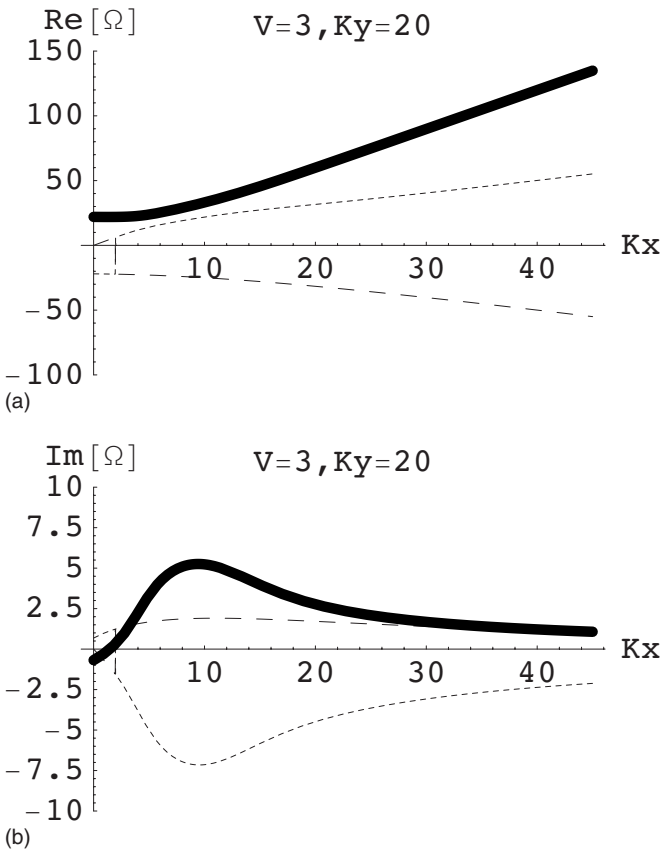

FIG. 2. (a) Real and (b) imaginary parts of the dispersion relation vs K_x for the case of $V=3$, $K_y=20$, $\beta_i=\beta_e=0.5$, and $\hat{\gamma}=1$.

This gives the dispersion relation for Ω. It is a third-order algebraic equation in Ω with three controlling parameters V, β_e, and β_i [$\mathcal{E}$ is not an independent parameter but is related to V by Eq. (4)]. We have

$$-\Omega^3 + K_x V\Omega^2 + (1 + K_y^2 + K_x^2 - 2\tau V^2)\Omega + \hat{\gamma}\frac{\beta_e}{2}(K_x^2 + K_y^2 - 4V^2)\Omega - K_x V\hat{\gamma}\frac{3\beta_e}{2}(K_x^2 + K_y^2) - K_x V\tau(1 + K_x^2 + K_y^2) + i[-K_y V(-1 + \tau + 2\hat{\gamma}\beta_e)\Omega + K_x K_y V^2(3\hat{\gamma}\beta_e + 2\tau)] = 0. \quad (19)$$

Figures 2(a) and 2(b) show the real and imaginary parts of the dispersion relation as a function of K_x for the case of $V=3$, $K_y=20$, $\beta_i=\beta_e=0.5$, and $\hat{\gamma}=1$ for all the three modes. To display the group velocity more clearly, Figs. 3(a) and 3(b) show the real and imaginary parts of the mode frequency as a function of K_y for the case of $V=3$, $K_x=15$, $\beta_i=\beta_e=0.5$, and $\hat{\gamma}=1$. Figure 3(c) shows the group velocities. One of the three modes has a very small group velocity. Figure 3(d) indicates the number of e-foldings of the three modes. Here, we define the e-folding number N as $N \equiv \mathrm{Im}[\Omega]/(V_{\mathrm{group}}\mathcal{E})$ and take it as an estimate of the number of e-foldings. We find the mode with the smallest group velocity also has the most e-foldings. It is the number of growths, while the mode passes the distance $1/\mathcal{E}$. In Sec. III, we discuss in some detail the importance of the small group velocity and the large number of e-foldings.

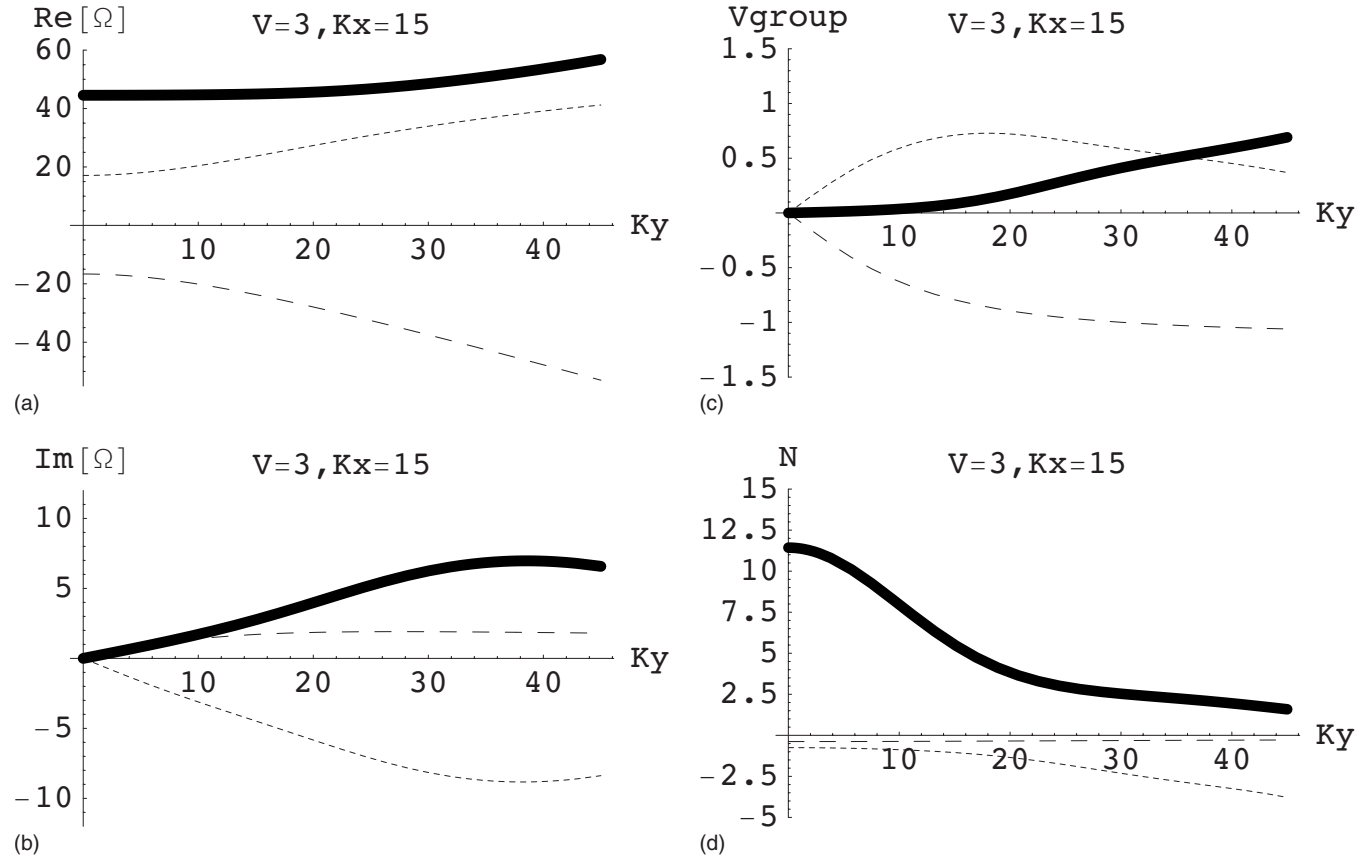

FIG. 3. (a) Real and (b) imaginary parts of the dispersion relation, (c) group velocities ($V_{\mathrm{group}} \equiv \partial\,\mathrm{Re}[\Omega]/\partial K_y$), and (d) e-foldings [$N \equiv \mathrm{Im}[\Omega]/(V_{\mathrm{group}}\mathcal{E})$] vs K_y for the case of $V=3$, $K_x=15$, $\beta_i=\beta_e=0.5$, and $\hat{\gamma}=1$.

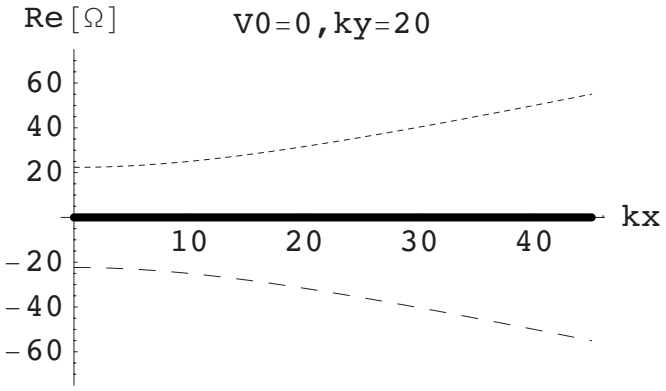

FIG. 4. Dispersion relation for the case that $V=0$, $\beta_e=\beta_i=0.5$, $\hat{\gamma}=1$, and $K_y=20$. There are two magnetosonic waves (dashed lines) and one beam wave (solid line).

III. WAVE CHARACTERISTICS AND INSTABILITY

Equation (19) gives Ω exactly for all the three modes. We now discuss the basic wave characteristics of the separate modes and the origin of the instabilities. We show how the exact modes can be conceived to be the simple wave modes coupled by linear interaction produced by the density gradient and current.

A. Waves without drift

First, we get a simple picture of the modes by examining the case that there is no drift. When $V=0$, Eq. (19) reduces to

$$-\Omega^3+\Omega(K_y^2+K_x^2)\left(1+\hat{\gamma}\frac{\beta_e}{2}\right)=0, \tag{20}$$

which represents two fast magnetosonic waves, and a modified entropy wave with $\Omega=0$, as shown in Fig. 4.

B. Instability

When $V\neq 0$, Eq. (19) still represents two fast magnetosonic waves as shown in Fig. 2. The modified entropy mode has become a beam mode (BM), $\Omega=\mathbf{K}\cdot\mathbf{V}$.

To get some insight into the modes' characteristics, we simplify Eq. (19) by assuming $K_y \gg K_x, V$, taking $\beta_e=0$, ($\tau=1$), and obtain

$$-\Omega^3+K_xV\Omega^2+(K_y^2-\tau\mathcal{E}_nV)\Omega-K_xVK_y^2+2iK_xK_yV^2=0. \tag{21}$$

Equation (21) can be factorized as

$$(\Omega-K_xV)(\Omega^2-K_y^2)+\tau\mathcal{E}V\Omega-2iK_xK_yV^2=0. \tag{22}$$

In Eq. (22), the first term clearly shows the three modes. One is a beam mode (BM, $\Omega=K_xV$), and the other two are magnetosonic modes (MS$^{\pm}$, $\Omega=\pm K_y$). The second and the third terms determine the modes' stability. It is worth noticing that both of these two terms depend on K_y and drift velocity V, which is directly related to equilibrium density gradient.

To get the analytical dispersion relations for the three modes, we solve Eq. (19) in different parameter regimes. First, we simplify Eq. (19) in the limit of large K and $\Omega\sim K$,

$$\Omega^2=(3\hat{\gamma}\beta_e+2\tau)\left(\frac{K_x^2+K_y^2}{2}-iVK_y\right). \tag{23}$$

These are the two magnetosonic waves.

For the beam wave, assuming large K and V but $\Omega\sim K\cdot V$, Eq. (19) then becomes

$$-\Omega^2+K_xV\Omega+(K_x^2+K_y^2)(1-\hat{\gamma}\beta_e-\tau)-\hat{\gamma}\frac{\beta_e}{2}\mathcal{E}^2+iK_yV(1+\tau+\hat{\gamma}\beta_e)=0. \tag{24}$$

Writing $\Omega=K_xV+\delta\Omega$, and solving for $\delta\Omega$, we obtain

$$\delta\Omega\approx\frac{K_x^2+K_y^2}{K_xV}(1-\hat{\gamma}\beta_e-\tau)-\hat{\gamma}\frac{\beta_e}{2}\frac{\mathcal{E}^2}{K_xV}+i\frac{K_y}{K_x}(1+\tau+\hat{\gamma}\beta_e). \tag{25}$$

Therefore, the dispersion relation of the beam mode is

$$\Omega\approx K_xV+\frac{K_x^2+K_y^2}{K_xV}(1-\hat{\gamma}\beta_e-\tau)-\hat{\gamma}\frac{\beta_e}{2}\frac{\mathcal{E}^2}{K_xV}+i\frac{K_y}{K_x}(1+\tau+\hat{\gamma}\beta_e). \tag{26}$$

The BM is represented by the solid curve in Figs. 2–4, while the MS$^{\pm}$ modes are given by the dotted and dashed curves.

We cannot be sure that the BM and MS$^{\pm}$ modes are unstable normal modes growing indefinitely. This is because we limit ourselves to a local theory and treat the modes as quasimodes. Strictly speaking, we should solve a differential equation in y to treat it properly. A quasimode could grow only a finite amount during propagation through the unstable region. However, as shown in Fig. 3(d), for the beam mode, the growth itself (N) is very large and the quasimode treatment should be adequate.

Perhaps it will make the quasi theory clearer if we compare with a sound mode in an inhomogeneous medium (see Appendix B). The sound mode increases adiabatically when propagating into decreasing density region but its growth can also be estimated from a quasimode similar to ours. The main difference is the much larger growth that our beam mode has.

The MS$^{\pm}$ modes have e-folding numbers about unity, which indicates these two modes may not be able to grow appreciably in the inhomogeneous media. Section III C will also show that the MS$^{\pm}$ modes would be stabilized by warm ion Landau damping anyway. Thus, only the BM could possibly be a real linear instability excited and growing in the Harris current sheet. In a following paper, we will discuss a nonlinear mode coupling mechanism that makes the MS$^{\pm}$ modes nonlinearly unstable. For the sake of simplicity, we will continue to call the three solutions of Eq. (19), modes in the following sections, although they may not be the normal ones.

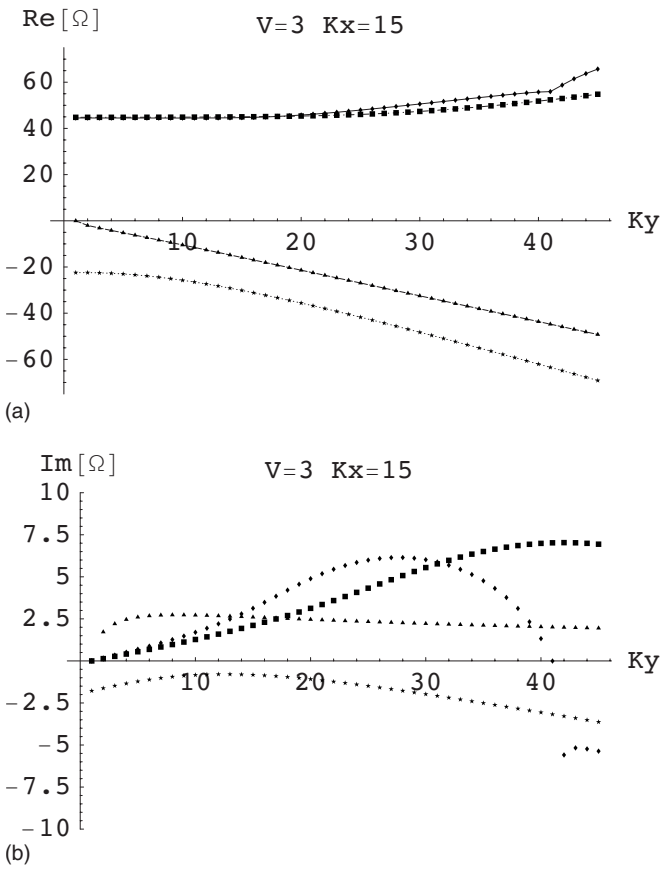

FIG. 5. (a) The real and (b) imaginary parts of the case of $K_x=15$, $V=3$, $\beta_e=0$, $\tau=1$, $\hat{\gamma}=1$ with warm ion effect. The squares show the cold BM and the diamonds give the warm BM. The triangles present the cold MS$^-$ and the stars show the warm MS$^-$. Clearly, the MS$^-$ is more affected by the warm ions and becomes a damping mode.

C. Warm ion effects

Before going into a detailed discussion of the instability mechanism, we show that warm ion effects suppress one of the unstable modes: the backward propagating magnetosonic mode. Instead of the cold ion equations (7) and (8), we use the warm ion equations (5) and (6) for the perturbed ion current and density and solve the dispersion relation. Figures 5(a) and 5(b) show the warm ion effects on the instabilities.

By comparing the cold ion and warm ion instabilities in Fig. 5(b), we see that the growth rates of the backward propagating magnetosonic waves are reduced by the warm ion Landau damping. However, the beam mode is hardly affected by the warm ions because its phase velocity is much higher than the ion thermal speed. From now on, we only concentrate on the unstable beam mode and discuss whether it could be a favorable candidate to exist in the center of the current sheet and produce anomalous resistivity in the MRX.

D. Instability mechanism

In this section, we will describe the mechanism of the beam instability. To get a clear physical picture, we redo the dispersion relation calculation in the electron frame. This eliminates the large leading term (K_xV) in the beam wave dispersion relation and reveals the feedback mechanism of the instability.

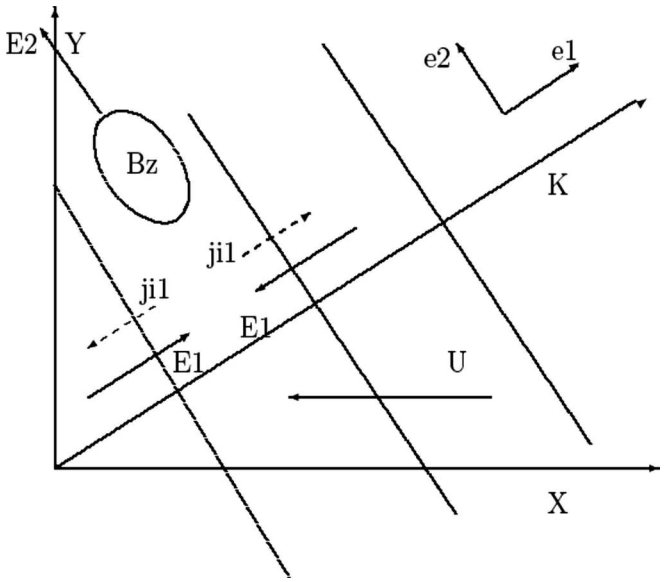

FIG. 6. Definitions of E_1 and E_2 in the electron frame. Ions drift toward the negative x direction, while electrons are at rest.

In the electron frame, the ions have a large drift velocity (Fig. 6). We will focus only on the $\beta_e=0$ case, which represents a clearer physical picture and does not change the generality since the pressure gradient is a higher order quantity compared to the electric and Lorenz forces. We take the $K, U \gg \Omega$ assumption to further simplify the algebra without losing the important physics. This is because the approximate dispersion relation of the beam mode [Eq. (26)] shows that the beam mode frequency after the Doppler shift ($\mathbf{K}\cdot\mathbf{V}$) is in the order of unity.

We rotate the coordinates for $\mathbf{E}$, as shown in Fig. 6. E_1 is the electrostatic component in the $\mathbf{k}$ direction. E_2 is the perpendicular component to $\mathbf{k}$ in the x-y plane, representing the electromagnetic component.

The perturbed equation for the electrons ($\hat{\gamma}=1$) now becomes

$$\mathbf{j}^e \times \mathbf{B}_0 = en_0\mathbf{E}. \tag{27}$$

In addition to the dimensionless parameters in Eq. (16), we further define other dimensionless quantities as

$$\hat{E} \equiv \frac{E}{V_A B_0}, \quad \hat{j} \equiv \frac{j}{en_0 V_A}, \quad \hat{n} \equiv \frac{n}{n_0}, \quad \hat{B} \equiv \frac{B}{B_0}. \tag{28}$$

With all the dimensionless parameters, the force equation on electrons [Eq. (27)] becomes in the $\mathbf{e}_1$ direction

$$\hat{E}_1 = \hat{j}_2^e \tag{29}$$

and in the $\mathbf{e}_2$ direction

$$\hat{E}_2 = -\hat{j}_1^e. \tag{30}$$

Similar to the calculation in the ion frame but with the finite drift velocity, we first calculate the perturbed ion velocity,

$$\frac{\partial \mathbf{v}}{\partial t} + \mathbf{U}\cdot\nabla\mathbf{v} = \hat{\mathbf{E}} + \mathbf{U}\times\hat{\mathbf{B}}, \tag{31}$$

$$\mathbf{v} \simeq i\frac{\hat{\mathbf{E}} + UB_z\hat{\mathbf{y}}}{KU\cos\theta}. \tag{32}$$

To get the perturbed density, we employ the continuity equation

$$\frac{\partial \hat{n}}{\partial t} + \mathbf{U}\cdot\nabla\hat{n} + \nabla\cdot\mathbf{v} = 0, \tag{33}$$

$$n \simeq \frac{\mathbf{K}\cdot\mathbf{v}}{KU\cos\theta}. \tag{34}$$

The perturbed ion current is

$$\hat{\mathbf{j}}_i = \mathbf{v} + \hat{n}\mathbf{U}, \tag{35}$$

From Eqs. (32) and (34), it is straightforward to calculate $\hat{\mathbf{j}}_i$,

$$\hat{j}_1^i = -\frac{\epsilon_n}{K^2U}\tan\theta E_1 - \frac{\epsilon_n}{K^2\cos\theta}B_z, \tag{36}$$

$$\hat{j}_2^i = i\frac{B_z}{K\cos^2\theta} + i\frac{K - i\epsilon_n}{K^2U}\tan^2\theta E_1 + \frac{\epsilon_n\sin\theta}{K^2\cos^2\theta}B_z. \tag{37}$$

The total perturbed current in $\mathbf{e}_1$ direction is zero (which is from charge neutrality, $\nabla\cdot\mathbf{j}=0$), and in $\mathbf{e}_2$ direction, the total current can be derived from Ampère's law,

$$\hat{j}_1^e + \hat{j}_1^i = 0, \tag{38}$$

$$\hat{j}_2^e + \hat{j}_2^i = -iK\hat{B}_z. \tag{39}$$

So far, we have all the perturbed quantities required to derive the dispersion relation of the beam mode in the electron frame. To reveal the key of the instability mechanism, we assume that $\hat{j}_2^i$ is negligible and we will show the self-consistency later. We then have the electron current

$$\hat{j}_2^e \simeq -iK\hat{B}_z. \tag{40}$$

From Eq. (29), we obtain an electrostatic field,

$$\hat{E}_1 = \hat{j}_2^e \simeq -iK\hat{B}_z. \tag{41}$$

This perturbed electric field $\hat{E}_1$ and magnetic field $\hat{B}_z$ drive an ion current in the $\mathbf{e}_1$ direction, as shown in Eq. (36). By charge neutrality, there is an equal and opposite signed electron current [see Eq. (36)].

Finally, as Eq. (30) shows, there must be an electromagnetic field $\hat{E}_2$,

$$\hat{E}_2 = -\hat{j}_1^e = \hat{j}_1^i. \tag{42}$$

So far, all the results apply at a fixed time. But because of Faraday's law, the electromagnetic fields $\hat{E}_2$ and $\hat{B}_z$ must change in time,

$$\frac{\partial \hat{B}_z}{\partial t} = -iK\hat{E}_2. \tag{43}$$

Combining Eqs. (43), (42), (41), and (40), we get

$$\frac{\partial \hat{B}_z}{\partial t} \simeq \epsilon_n\left(\frac{\tan\theta}{U} + i\frac{1}{K\cos\theta}\right)\hat{B}_z. \tag{44}$$

Because the imaginary term is positive, $\hat{B}_z$ and all the other perturbed quantities grow in time. This result is identical with the BM dispersion relation [Eq. (26)] in the ion frame by setting $\beta_e=0$.

By combining Eqs. (43), (42), (41), and (40), we also see the self-consistency of our previous assumption. That $\hat{B}_z$ is much smaller than $\hat{E}_1$ goes with the assumption that $\hat{j}_2^i$ is negligible.

Summarizing the physical process, we start with a perturbed magnetic field. For this fixed time, a perturbed ion current in the $\mathbf{k}$ direction requires an equal and opposite signed electron current in the same direction. This electron current needs an electromagnetic field E_2 to achieve the force balance on electrons in the $\mathbf{e}_2$ direction. Since E_2 and B_z must change in time by Faraday's law, we develop the positive feedback loop for the magnetic field B_z, and for the other perturbed quantities as well.

Briefly speaking, the ion flux in the $\mathbf{k}$ direction caused by finite density gradient ϵ_n, initiates the positive feedback process and triggers the instability.

IV. INSTABILITY IN THE HARRIS SHEET

It is important to see how the nonlocal modes behave in a finite current layer. For this purpose, we consider a Harris sheet. In this section, we will emphasize the importance of the two characteristics of the beam mode: its growth rate and its group velocity across the current layer. The growth rate is obviously important since it determines how fast the mode grows. However, we find the group velocity across the current layer is equally, if not more, important. To see this, we apply our theory to the Harris current sheet,

$$B = B_0\tanh\frac{y}{\delta} \equiv B_0 t,$$
$$n = n_0\sec^2\frac{y}{\delta} \equiv n_0(1-t^2), \tag{45}$$

where $t \equiv \tanh(y/\delta)$.

In the Harris sheet, in Eq. (19), we replace the local parameters by global parameters as shown in Eq. (46),

$$K \to \frac{K}{\sqrt{1-t^2}}, \quad \mathcal{E} \to \frac{\mathcal{E}}{\sqrt{1-t^2}}, \quad V \to \frac{\sqrt{1-t^2}}{t}V,$$
$$\beta \to \frac{1-t^2}{t^2}\beta, \quad \Omega \to \frac{\Omega}{t}. \tag{46}$$

The dimensionless parameters are defined as in Eq. (16). We use the maximum n_0, B_0 of the Harris sheet profile instead of local n, B to define $\omega_{ci0}, V_{A0}, \omega_{pi0}$. This avoids the confusion when switching to dimensional parameters from dimensionless expressions.

For the obliquely propagating instabilities, the modes have a group velocity on the order of the Alfvén speed across

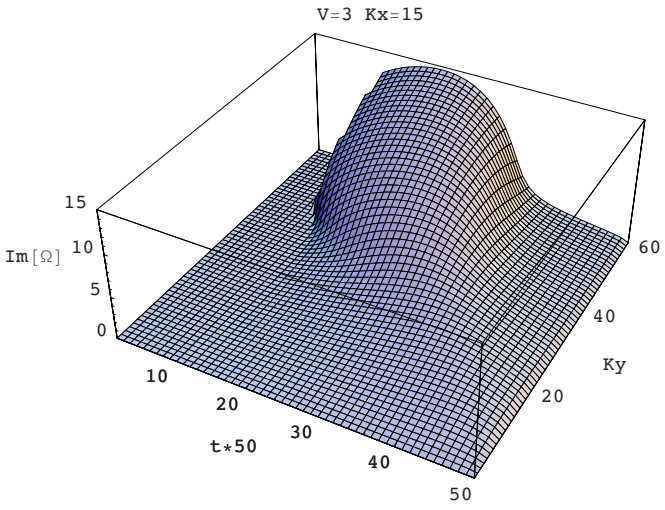

FIG. 7. (Color online) The growth rate of the beam mode in the Harris sheet, $V=3$, $K_x=15$.

the current sheet. These modes only make one e-folding before they propagate out of the unstable region, which means they do not have enough time to grow to the desired amplitude in spite of their large growth rates (Appendix A). However, from Eq. (26), we can see that the dominant term of Ω does not depend on K_y, which means the beam mode has a very small group velocity in the y direction: $V_{\text{group}} \equiv \partial \text{Re}[\Omega]/\partial K_y$. Figure 7 shows the beam mode for the case of $V_0=3$, $K_x=15$ in the Harris current sheet. Figure 8 shows the beam mode at $t=0.7$, which corresponds to a point halfway to the center of the Harris current sheet, the group velocity in the y direction, and the e-foldings N [$N \equiv \text{Im}[\Omega]/(V_{\text{group}}\mathcal{E})$]. Because of the extremely small group velocity in the y direction, the beam modes probably have sufficient e-foldings to reach a nonlinear state before they propagate out of the unstable region. This makes the beam mode more promising when we consider modes that produce enhanced resistivity.

Using the dimensionless global parameter $\beta \rightarrow 1 - t^2/t^2\beta$ [Eq. (46)], we obtain the group velocity

$$V_g = \frac{2K_y}{K_x V}\left(2 - \frac{1}{t^2}\right)\beta_{e0} \tag{47}$$

and the e-foldings

$$N = \frac{V(t^2 + \beta_{e0})}{2(2t^2 - 1)\beta_{e0}}. \tag{48}$$

Equation (47) gives a very special location in the Harris sheet, i.e., $t=1/\sqrt{2}$, where $V_g=0$. For all the $\beta_{0e}+\beta_{0i}=1$ cases (which is always true because we assume there is no background density, which gives $P_0=B_0^2/2\mu$), the $V_g=0$ location is the same. Since the $V_g=0$ point is an interesting

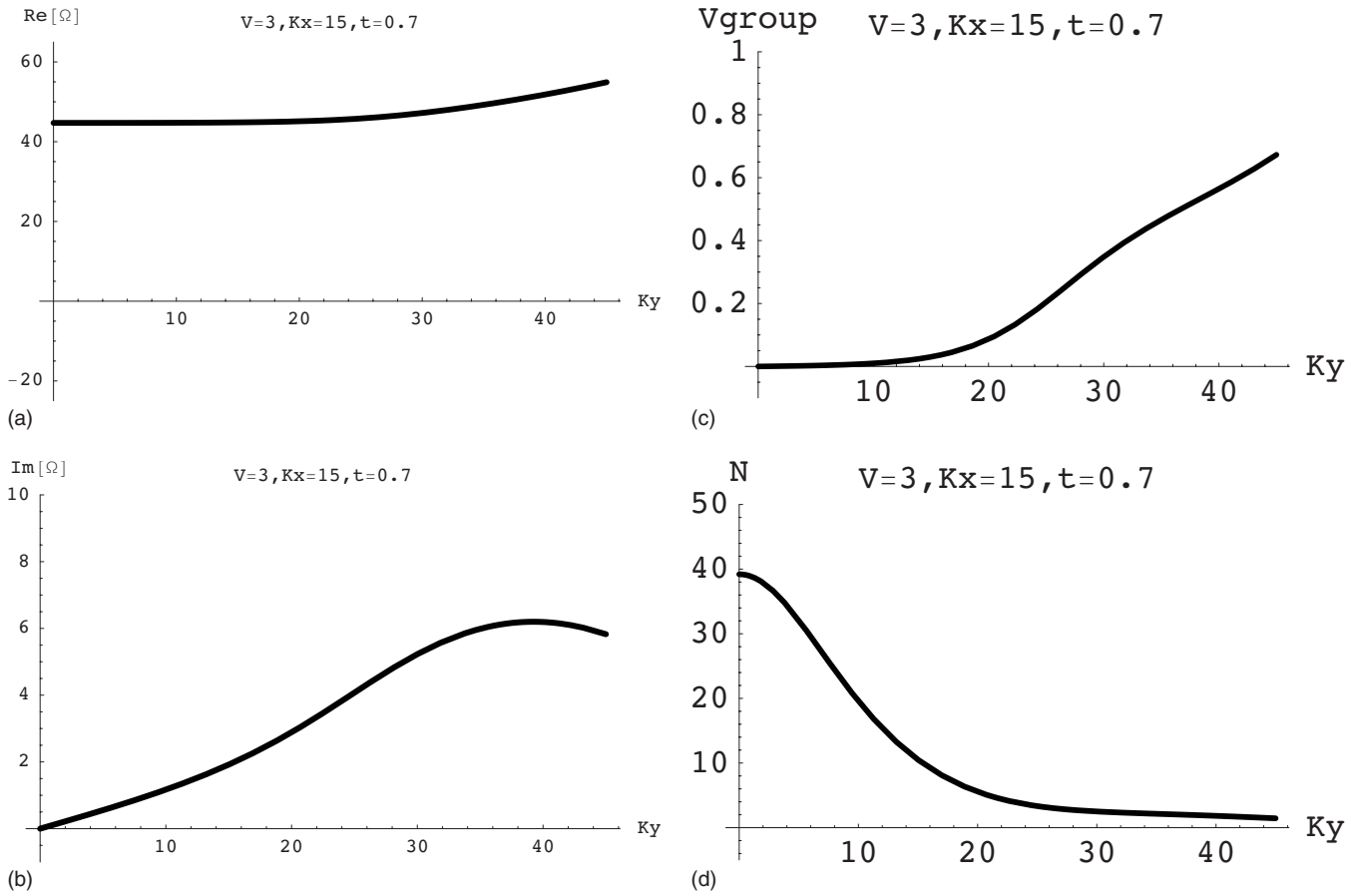

FIG. 8. (a) The frequency, (b) the growth rate, (c) the group velocity, and (d) the e-foldings of the beam mode at the halfway to the center of the Harris sheet, $t=0.7$, $V=3$, $K_x=15$.

location where the instability can stay and grow for a long time, it could be a source of the instabilities in the current layer.

V. THE EFFECT OF ELECTRON-ION COLLISIONS

As discussed in Sec. II, we rely on a modest electron-electron collision rate to satisfy the isotropic (isothermal or adiabatic) electron pressure assumption and the neglect of the ∇B drift Landau damping. However, we have not kept electron-ion collisions in the electron force balance equation (9). Now, if we add electron-ion collisions (i.e., resistivity) to the electron motions, the new electron force balance equation is given by

$$\mathbf{j}^e \times \mathbf{B}_0 = en_0 V_0 \times \mathbf{B} + en_0 \mathbf{E} + en\mathbf{E}_0 + \hat{\gamma}\nabla(n_1 T_e) + mn_0 \nu_{ei} \frac{\mathbf{j}^{\text{total}}}{e}. \tag{49}$$

After some algebra, we obtain the revised matrix to calculate dispersion relations

$$\begin{pmatrix} D_{xx} & D_{xy} \\ D_{yx} & D_{yy} \end{pmatrix} \begin{pmatrix} E_x \\ E_y \end{pmatrix} = 0, \tag{50}$$

where

$$D_{xx} = 1 + K_y^2 - \tau \frac{K_x V}{\Omega} + iVK_y - i\hat{\gamma}\frac{\beta_e}{2}\frac{K_x(K_y - i\hat{\epsilon})}{\Omega} + \frac{m}{M}\hat{\nu}_{ei}K_x K_y,$$

$$D_{xy} = i(\Omega - K_x V) - \tau \frac{K_y - i\hat{\epsilon}}{\Omega} V - i\hat{\gamma}\frac{\beta_e}{2}\frac{(K_y - i\hat{\epsilon})^2}{\Omega} - K_x K_y - \frac{m}{M}\hat{\nu}_{ei}K_x^2,$$

$$D_{yx} = i\hat{\gamma}\frac{\beta_e}{2}\frac{K_x^2}{\Omega} - i\Omega - K_x K_y,$$

$$D_{yy} = 1 + K_x^2 + i\hat{\gamma}\frac{\beta_e}{2}\frac{K_x(K_y - i\hat{\epsilon})}{\Omega} + \frac{m}{M}\hat{\nu}_{ei}K_y^2.$$

Here, $\hat{\nu}_e \equiv \nu_{ei}/\omega_{ci}$ is the new dimensionless parameter.

To find the beam mode, the same as Sec. II, we assume large K and V with $\Omega \sim K \cdot V$. Similar to Eq. (26), the approximate dispersion relation of the beam mode with collisions is given by

$$\Omega \approx K_x V + \frac{K_x^2 + K_y^2}{K_x V}(1 - \hat{\gamma}\beta_e - \tau) - \hat{\gamma}\frac{\beta_e}{2}\frac{\mathcal{E}^2}{K_x V} + i\left[\frac{K_y}{K_x}(1 + \tau + \hat{\gamma}\beta_e) - \frac{m}{M}\hat{\nu}_{ei}(K_x^2 + K_y^2)\right]. \tag{51}$$

The imaginary part has two terms: one gives the wave growth rate, which is the same as the collisionless calculation; the other term arises from the electron-ion collisions damps the modes. The damping rate depends on collisional rates and wave vectors. The sum of these two effects gives the final growth rate of the beam mode. From Eq. (51), we see that the larger β_e, K_y but smaller K_x will make the imaginary part positive. The unstable modes appear near the center of the current sheet where β_e is large. The small K_x modes are more unstable. Physically, the electron-ion collisions are a mechanism that resistively diffuses the perturbed magnetic field at the rate $K^2\eta$, which for large K spreads out the mode and tends to stabilize it.

VI. DISCUSSION AND CONCLUSIONS

A. Discussion

In this paper, we only study the electromagnetic modes. We are interested the modes that can be excited in the center of the current sheet, but the pure electrostatic modes do not exist in this high plasma β region because the perturbed magnetic field is proportional to the plasma β and the perturbed density. In the MRX, electrostatic fluctuations were found by Carter *et al.* However, it turned out these fluctuations only exist on the edge of the current sheet where β is small and do not correlate well in time with the reconnection process. Later, electromagnetic fluctuations were found in the center of the current sheet and correlate in time with the reconnection progress.

Compared with the previous oblique LHDI mode,[23] which has a large group velocity and smaller phase velocity than the experimental data, the perpendicularly propagating unstable beam mode which we describe here has several favorable characteristics. It has a very small group velocity across the unstable region in the current layer. The obliquely propagating instability has about one or two e-foldings, but the perpendicular one has tens of e-foldings. This instability is not affected by the warm ion effect because of the large phase velocity. The growth rate of the oblique LHDI is reduced to half when including the warm ion effect. The growth rate of this unstable beam mode is not sensitive to its location in the current sheet. The oblique LHDI has a very narrow unstable region in the Harris sheet.

In the previous LHDI calculations, the instability arises from the finite $k_\perp \rho_e$ effect and is saturated in the high β region because of the ∇B drift resonance. But in the MRX, the electron-electron and electron-ion collisions are not negligible and even the modest collision rates can disturb the ∇B drift resonance. Thus, the ∇B drift resonance cannot damp the instability in the MRX. Further, if the collision rate is high enough, the finite $k_\perp \rho_e$ effect cannot play an important role and the plasma behaves more like a fluid.

During the formation of the current layer, as it becomes narrower, the drift velocity becomes larger. It is still not clear why the current layer stops shrinking at some critical widths. A possible explanation is that some instability is excited when the drift velocity becomes large enough. This instability can enhance the resistivity and trigger the fast reconnection. At the same time it can stop the shrinking of the current layer by providing enhanced resistivity. Based on the experimental results, we assume a large drift velocity. Since the density gradient and drift velocity are related, we also keep the equilibrium density gradient term in the perturbed

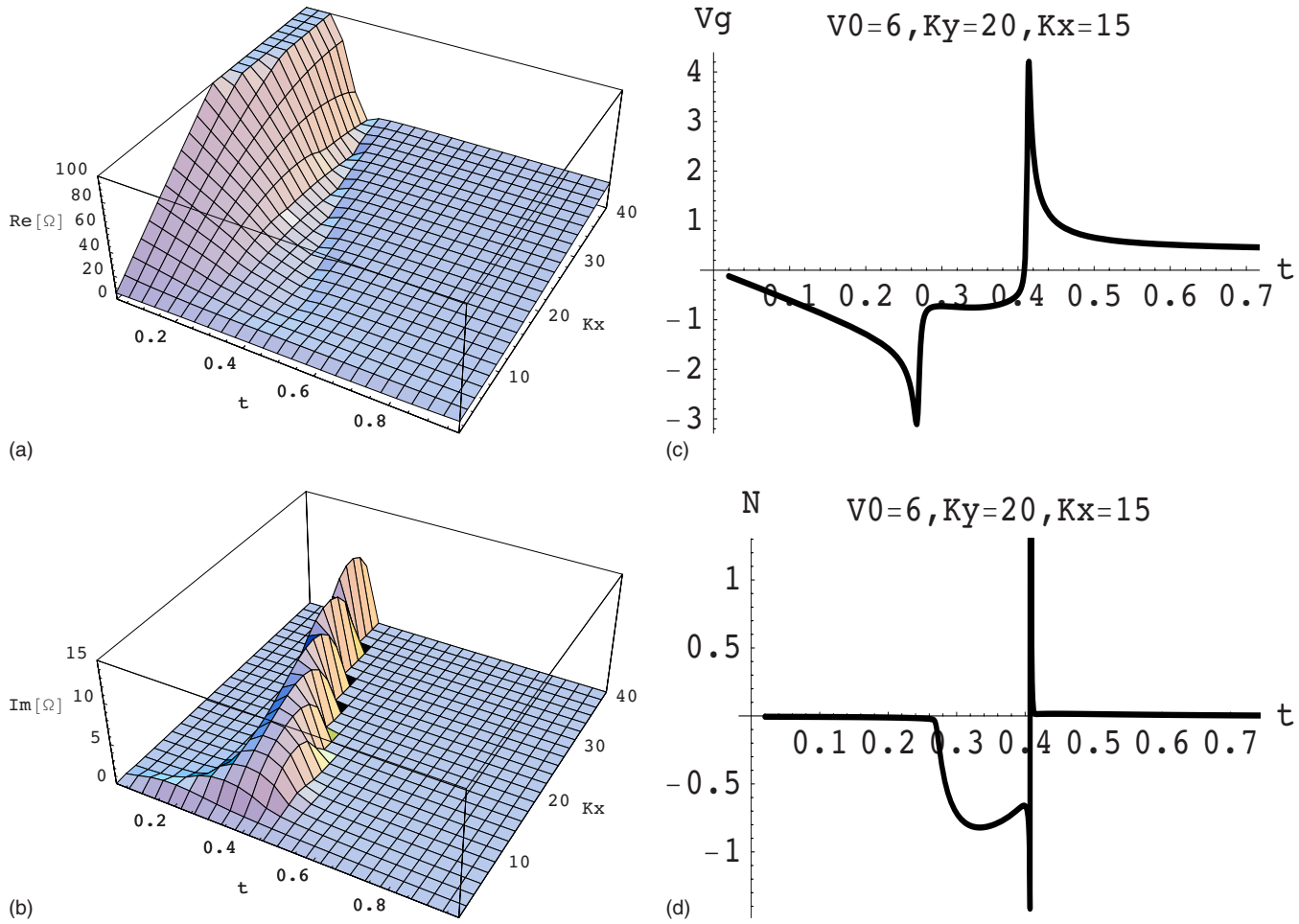

FIG. 9. (Color online) (a) The dispersion relation and (b) the growth rate for $V=6$, $K_y=20$ mode, and $\beta_{e0}=\beta_{i0}=0.5$. (c) The group velocity and (d) number of e-foldings of the obliquely propagating instability as a function of $t=\tanh(y/\delta)$ for $V=6$, $K_y=20$, $K-x=15$ and the same β_e, β_i.

density and the pressure. This density gradient is one of the two factors that trigger the instability; the other one is the finite k_y.

B. Conclusions

We have developed a local theory to derive and analyze in detail an unstable electromagnetic beam wave that propagates perpendicularly to the unperturbed magnetic field. This instability has a small group velocity across the current layer and a large number of e-foldings before it leaves the unstable region. Because of the large electron streaming velocity in the current layer, the phase velocity of the drift instability is much higher than the ion thermal speed. This means that the warm ion Landau damping does not stabilize this drift instability. Thus, this instability is a favorable candidate to enhance the resistivity within the reconnection layer.

We also identify that the instability arises from a positive feedback mechanism triggered by the nonzero ion flux in the **k** direction resulting from the finite density gradient.

In Sec. II, we assume that the electrons are isothermal or adiabatic because there are enough electron-electron collisions in the MRX. In Sec. V, we add a finite electron-ion collision (resistivity) term to the electron force balance equation (49). We find that the electron-ion collisions diffuse the perturbed magnetic field at the rate of $k^2\eta$, but for small k_x, large k_y and large β_e, the drift instability is still unstable and could grow to a sufficient amplitude to produce the enhanced resistivity.

Our theory is self-consistent in that the density gradient ϵ and drift velocity V_0 are related by the equilibrium equations. The instability we find is thus related to the LHDI. Our theory has the potential to explain the experimental results from the MRX, and possibly provides an understanding of fast reconnection mechanism. In the next paper we will develop a nonlinear theory to determine saturated amplitudes and their consequences for reconnection.

ACKNOWLEDGMENTS

The comparison of the sound mode in an inhomogeneous medium with our beam mode was suggested by the referee. We would like to thank him/her for this input, which makes our theory clearer and more complete.

APPENDIX A: APPLICATION OF THE OBLIQUELY PROPAGATING INSTABILITY TO THE HARRIS CURRENT SHEET

An obliquely propagating electromagnetic instability in the lower hybrid frequency range has been investigated in detail by Ji *et al.*[23] They term the instability as the oblique LHDI. Here, we add K_y into the calculation and apply to the Harris current sheet. Figure 9 shows the growth rate, group velocity, and number of e-foldings for the instability of $V=6$, $\beta_e=\beta_i=0.5$, and $\theta=60°$. Here, θ is the angle between $\hat{z}$ and $\hat{k}$.

From Fig. 9, we see that the oblique LHDI has a large group velocity in y direction. Thus, the oblique LHDI has very few e-foldings, which makes the instability not very likely to be able to grow to the desired amplitude that brings in the nonlinear effect.

APPENDIX B: REAL INSTABILITY OR NOT?

In Sec. III B, we mention that our instability (BM) may not be a normal mode but a real quasimode instability. Here, we compare our treatment of the BM with a parallel treatment of the sound mode in an inhomogeneous medium.

The dispersion relation of a sound mode in the inhomogenous media is

$$\omega^2 = c_s^2 k_y (k_y - i\epsilon). \tag{B1}$$

For fixed k_y, the mode has a growth rate of $\Gamma=c_s\epsilon/2$. The mode could increase exponentially but only at a rate related to the inhomogeneity scale. This can be interpreted as the correct behavior of a sound wave, since by energy conservation, $nmv^2/2$ is a constant and n increases at the rate $e^{\epsilon y}$.

In terms of our calculation of mode e-folding numbers, one can estimate the amount of growth of the sound mode over the scale height $1/\epsilon$, as of order

$$N \equiv \frac{\Gamma}{v_g \epsilon} = \frac{c_s \epsilon/2}{c_s \epsilon} = \frac{1}{2}, \tag{B2}$$

which agrees with the energy argument.

Figure 3(d) shows that N is much larger than unity for the BM, so the BM must amplify the electric field by a substantial amount when passing though a inhomogeneity distance and should be a substantial instability. While the $MS^{\pm}$ modes have N about 1, they may not really exist in the inhomogeneous media linearly.

A more correct way to treat the instabilities is to solve for k at fixed real ω (which has an imaginary part $\epsilon/2$ for the sound mode case). For the sound mode, the imaginary part of k/ϵ is exactly equal to the N of our estimate. However, for a strongly growing mode (large N), this formula is not strictly valid.

For our large k beam modes, given k_x and ω, from Eq. (26) but with $\beta_e=0$ and $\tau=1$,

$$K_y \approx -i\frac{K_x}{2}(\Omega - K_x V), \tag{B3}$$

which can be very large for a proper choice of Ω.

[1] M. Yamada, H. Ji, S. Hsu, T. Carter, R. Kulsrud, N. Bretz, F. Jobes, Y. Ono, and F. Perkins, Phys. Plasmas **4**, 1936 (1997).
[2] R. Ren, M. Yamada, S. Gerhardt, H. Ji, R. Kulsrud, and A. Kuritsyn, Phys. Rev. Lett. **95**, 055003 (2005).
[3] R. Kulsrud, H. Ji, W. Fox, and M. Yamada, Phys. Plasmas **12**, 082301 (2005).
[4] H. Ji, S. Terry, M. Yamada, R. Kulsrud, A. Kuritsyn, and Y. Ren, Phys. Rev. Lett. **92**, 115001 (2004).
[5] P. Sweet, in *Electromagnetic Phenomena in Cosmical Physics*, edited by B. Lehnert (Cambridge University Press, New York, 1958), p. 123.
[6] E. Parker, J. Geophys. Res. **62**, 509, DOI: 10.1029/JZ062i004p00509 (1957).
[7] H. Petschek, *AAS–NASA Symposium on the Physics of Solar Flares*, NASA Spec. Publ. Sp-50 (NASA, Washington, D.C., 1964), p. 425.
[8] T. Carter, M. Yamada, H. Ji, R. Kulsrud, and F. Trintchouk, Phys. Plasmas **9**, 3272 (2002).
[9] T. A. Carter, Ph.D. thesis, Princeton University, 2001.
[10] W. Daughton, Phys. Plasmas **10**, 3103 (2003).
[11] N. A. Krall and P. C. Liewer, Phys. Rev. A **4**, 2094 (1971).
[12] N. T. Gladd, Plasma Phys. **18**, 27 (1976).
[13] R. Davidson, N. Gladd, C. Wu, and J. Huba, Plasma Phys. **20**, 301 (1977).
[14] J. Huba, J. Drake and N. Gladd, Phys. Fluids **23**, 552 (1980).
[15] D. Winske, Phys. Fluids **24**, 1069 (1981).
[16] P. Yoon and A. Lui, Phys. Fluids B **5**, 836 (1993).
[17] P. Yoon, A. Lui and C. Chang, Phys. Plasmas **1**, 3033 (1994).
[18] P. Yoon, A. Lui, and M. Sitnov, Phys. Plasmas **9**, 1526 (2002).
[19] P. Yoon and A. Lui, J. Geophys. Res. **109**, A02210 DOI: 10.1029/2003JA010180 (2004).
[20] C. Wu, Y. Zhou, S. Tsai and S. Guo, Phys. Fluids **26**, 1259 (1983).
[21] T. Stix, *Waves in Plasmas* (American Institute of Physics, New York, 1992).
[22] R. Kulsrud, *Plasma Physics for Astrophysics* (Princeton University Press, Princeton, 2005).
[23] H. Ji, R. Kulsrud, W. Fox, and M. Yamada, J. Geophys. Res. **110**, A08212, DOI: 10.1029/2005JA011188 (2005).